Scientific Reports

https://doi.org/10.1038/s41598-026-68201-6

Article in Press

Regime shift in high arctic fjord signals the vulnerability of the Arctic's Last Ice Area

Received: 13 March 2026

Accepted: 20 August 2026

Published online: 27 August 2026

Cite this article as: Bonneau J., Hamilton A.K., Mueller D. *et al.* Regime shift in high arctic fjord signals the vulnerability of the Arctic's Last Ice Area. *Sci Rep* (2026). https://doi.org/10.1038/s41598-026-68201-6

J. Bonneau, A. K. Hamilton, D. Mueller, B. E. Laval, A. L. Forrest, A. J. Crawford, Y. K. Antropova, J. Shoapik, S. Pijamini & W. F. Vincent

We are providing an unedited version of this manuscript to give early access to its findings. Before final publication, the manuscript will undergo further editing. Please note there may be errors present which affect the content, and all legal disclaimers apply.

If this paper is publishing under a Transparent Peer Review model then Peer Review reports will publish with the final article.

ARTICLE IN PRESS

© The Author(s) 2026. **Open Access** This article is licensed under a Creative Commons Attribution-NonCommercial-NoDerivatives 4.0 International License, which permits any non-commercial use, sharing, distribution and reproduction in any medium or format, as long as you give appropriate credit to the original author(s) and the source, provide a link to the Creative Commons licence, and indicate if you modified the licensed material. You do not have permission under this licence to share adapted material derived from this article or parts of it. The images or other third party material in this article are included in the article's Creative Commons licence, unless indicated otherwise in a credit line to the material. If material is not included in the article's Creative Commons licence and your intended use is not permitted by statutory regulation or exceeds the permitted use, you will need to obtain permission directly from the copyright holder. To view a copy of this licence, visit http://creativecommons.org/licenses/by-nc-nd/4.0/.

ARTICLE IN PRESS

Journal: Nature Scientific Reports
Title: Regime Shift in High Arctic Fjord Signals the Vulnerability of the Arctic's Last Ice Area
Authors: J Bonneau[1,2,*], A K Hamilton[3], D Mueller[4], B E Laval[2], A L Forrest[5,6], A J Crawford[7], Y K Antropova[4], J Shoapik[8], S Pijamini[8], W F Vincent[9,10]

1. Department of Civil and Water Engineering, Université Laval, Quebec City, Canada
2. Department of Civil Engineering, The University of British Columbia, Vancouver, Canada
3. Department of Earth and Atmospheric Sciences, University of Alberta, Edmonton, Canada
4. Department of Geography and Environmental Studies, Carleton University, Ottawa, Canada
5. Department of Civil and Environmental Engineering, UC Davis, Davis, United States of America
6. Tahoe Environmental Research Center, UC Davis, Davis, United States of America
7. School of Life and Environmental Sciences, University of Stirling, Stirling, United Kingdom
8. Ausuittuq (Grise Fiord), Nunavut, Canada
9. Department of Biology & Takuvik Joint International Laboratory, Université Laval, Quebec City, Canada
10. Centre for Northern Studies, Université Laval, Quebec City, Canada

*Corresponding author: jeremie.bonneau@gci.ulaval.ca

Abstract

A consequence of the collapse of Arctic ice shelves is the draining and loss of epishelf lakes and their unique ice-dependent ecosystems. Epishelf lakes are formed by meltwater runoff that is dammed behind an ice shelf resulting in a perennial layer of freshwater (or lake), floating directly on seawater. They were once widespread in the Arctic and have been present for thousands of years. After several drainage events across the region, the last epishelf lake in the Canadian Arctic was lost during the collapse of the Milne Ice Shelf in 2020. We assess the range of oceanographic, atmospheric, and cryospheric factors that likely contributed to this major calving event, and analyze an unprecedented record of epishelf lake drainage from an ice-tethered mooring. A decadal timeseries of water column profiles collected pre- and post-calving show the abrupt one-way transition from a relatively stable freshwater ecosystem to a marine system. The loss of the Milne Fiord epishelf lake marks the extinction of a rare feature of a colder world and highlights the vulnerability of even the 'Last Ice Area' of Arctic sea ice to climate warming.

1. Introduction

The Last Ice Area (LIA) along the coastal margin of northern Canada and Greenland is considered a sea-ice refuge for wildlife in the face of global warming, and it contains diverse ecosystem types that depend upon ice integrity [1,2]. Among such ice-dependent features are epishelf lakes, perennial layers of freshwater directly overlying seawater that form from the accumulation of meltwater runoff in a fjord or inlet behind an ice shelf. In the 20th century, between 10 and 17 epishelf lakes occurred behind individual ice shelves along the north coast of Ellesmere Island [3] (Figure 1). These highly stratified polar ecosystems contain remarkable freshwater and marine biota in the same water column [4-6]. Epishelf lake systems have, however, been increasingly lost through ice shelf break-up and drainage [3,7] (Figure 1).

The last epishelf lake in Canada was in Milne Fiord, behind the 186.2 ± 0.4 km^2, up to 85 m thick, Milne Ice Shelf (MIS; Figure 2a), northern Ellesmere Island. The former epishelf lake in nearby Disraeli Fiord was thought to have existed for most of the last 4000 years [8]. The Milne Fiord epishelf lake harbored an extremely rare ecosystem type, with unique assemblages of freshwater and marine plankton and ice-associated biota [1,9]. The epishelf lake was 18 m deep when discovered in 1983 but had shoaled to a depth of ~10 m by 2011 from the MIS thinning [10]. Continuous monitoring of the lake from 2011 onward revealed seasonal oscillations in lake depth resulting from a net positive balance during periods of meltwater inflow followed by net drainage below the ice shelf over winter [10,11]. The outflow pathway was identified as a narrow basal channel that bisected the ice shelf (Figure 2a). The channel was sharply incised into the ice shelf

ARTICLE IN PRESS

leaving, at most, 10 m of ice above the channel apex [12,13], which controlled the depth of the epishelf lake.

In late July 2020, the MIS, the largest remaining stable ice shelf along the northern coast of Ellesmere Island, suffered a major calving event. In this study, we combine data from multiple sources, including remote sensing imagery and in-situ mooring and water column profiling, to evaluate the potential drivers of the ice shelf calving event, identify the mechanisms of the drainage of the freshwater lake, and describe the loss of this rare ecosystem.

2. Milne Ice Shelf Calving

Calving began between 30 and 31 July 2020 along pre-existing fractures. This included a dormant rift, which formed sometime prior to 1959 [14] and extended from the eastern ice shelf margin to the basal channel, and a more recent fracture that ran from the basal channel to the western margin (NW fracture; Figure 2 and 3). This calving created a 64.9±0.6 km^2 tabular iceberg with a mean thickness of 64±2.9 m, which quickly split along the basal channel into two ice islands of 54.0±0.4 km^2 and 10.9±0.2 km^2 (Figure 3b). A 18.6±0.6 km^2 thinner (47±2.9 m) portion of the ice shelf disintegrated into small pieces (Figure 3b,f). During the calving event, the outer section of the basal channel was lost and the status of the epishelf lake became uncertain. The remaining ice shelf had a surface area of 102.7±0.3 km^2; 45% was lost.

3. Loss of the Milne Fiord Epishelf Lake

Salinity profiles and moored observations from Milne Fiord document the deterioration and eventual loss of the epishelf lake. Prior to 2018, the near-surface salinity of the lake remained <1 g kg^{-1} (Figure 4a,b), and between 2011 and 2018, the depth of the epishelf lake, defined by the halocline separating freshwater (<1 g kg^{-1}) from seawater (>25 g kg^{-1}), was relatively stable at 8–12 m (Figure 4a,c). However, near-surface salinity first exceeded 1 g kg^{-1} in November 2018, suggesting that the integrity of the ice dam may already have been compromised. Although the lake continued to freshen and deepen during summer 2019, salinity increased and exceeded 2 g kg^{-1} during winter 2019/20 (Figure 4b). Following the calving event in July 2020, near-surface salinity began increasing in mid-summer (Figure 4b) despite elevated meltwater inflow (Figure 5c), indicating that freshwater export had become larger than meltwater inflow. Salinity increased rapidly after meltwater inflow ceased in September, and surface waters remained >1 g kg^{-1} thereafter. The first post-calving salinity profile collected in July 2022 showed that the halocline had shoaled to 2.4 m and that the distinct freshwater layer had been replaced by brackish conditions. While there is an observational gap between the last mooring salinity observation in March 2021 and the July 2022 profile, the rapid and early salinity increase in autumn 2020 indicates that the epishelf lake had mostly drained into the Arctic Ocean by then. Profiles collected annually since 2022 showed no evidence of re-establishment of the freshwater layer. Because the surface mass balance of the glaciers surrounding the fjord remained similarly negative to previous years (Figure 5c), reduced freshwater input is unlikely to explain this persistent absence. Instead, these observations suggest that freshwater entering the fjord is directly flushed to the ocean because the ice shelf has not regained the structural integrity required to retain it.

Given the lake began draining immediately after the calving event, the epishelf lake dam (i.e. the thickest roof ice along the channel apex) must have been located in the outer portion of the ice shelf and lost during calving (Figure 6). Notably, summer field observations in 2022 showed the roof of the remaining section of the channel had collapsed, becoming a ~30 m-wide open river draining freshwater to the ocean (Figure 6b). Available satellite imagery shows the channel roof collapsed prior to April 2021 (with open water visible in the channel in September 2021; Figure

ARTICLE IN PRESS

3d), implying it collapsed not long after the calving event and ice blocks melted or were carried away by the fjord surface water outflow.

4. Possible Causes of the Ice Shelf Break Up

In this section we examine the possible causes for the calving of MIS. First, we look at the preconditioning mechanisms that, over the last decades, have placed the MIS in a vulnerable position. We then review the possible triggering mechanisms that may have initiated the calving at the end of July 2020.

Preconditioning Factors:

a. Pre-existing structural weaknesses

Ice shelf elevation above sea level from ArcticDEM [15] revealed that despite relatively thick ice over the outer portion of the ice shelf (mean 64 m, see methods), the MIS had multiple pre-existing structural weaknesses (Figure 2): 1) the basal channel with a maximum thickness of ~7 m where warm water flowed from the epishelf lake to the ocean, 2) the dormant rift on the NE section with ice thickness less than 5 m, 3) a relatively new fracture in the NW section, and 4) relatively thinner ice in the troughs of the ice shelf's rolling surface. The basal channel and the dormant rift are visible in aerial imagery from 1959 (Figure 2b), while the NW fracture appeared during the winter of 2013.

b. Negative surface mass balance

The MIS had been in a state of negative surface ice mass balance since 1981, with an average surface mass balance of 0.30 m w.e.a^{-1}, with higher values around -0.16 w.e.a^{-1} for the calved section because of the colder air temperature seaward during summer [16,17]. The surface ablation of the two glaciers on each side of Milne Fiord's mouth reached a record mass loss of -0.45 m w.e.a^{-1} in 2019 and was highly negative again in 2020 (-0.38 m w.e.a^{-1}; Figure 5c) indicating there was no sign of recovery in the years prior to calving.

c. Distributed basal melting

The oceanographic mooring showed that the ocean temperature at 45 m depth, which was the average thickness of the ice shelf, was on average -1.5ºC (0.2 to 0.3ºC above freezing) over 2011 to 2020. This resulted in slow but continuous basal melting for a decade prior to the calving event. Recent modeling over the 2011 to 2019 period estimated the basal melting of the calved section to be 0.1 m w.e. a^{-1} [18].

Ice-shelf thinning is recognized as a pre-conditioning factor leading to failure, with ocean-driven basal melt being the main culprit across many Arctic and Antarctic contexts [e.g. 19]. Thinning, along with pre-existing and accumulating damage, leave ice shelves weakened and unable to withstand elevated stress resulting from, for example, compression against pinning points [20], enhanced flexure from ocean swell [19,21,22] or accumulated surface melt ponding [23].

Triggering Factors:

d. Basal Channel melting

The elevated air temperatures and surface melt in 2019 and 2020 resulted in enhanced freshwater inflow to the epishelf lake and therefore higher outflow velocities in the basal channel (Figure 5c,d). In addition, the mooring observations showed that 2020 had the warmest water temperature at 5 m depth in the lake (Figure 5a). Observations along the basal channel showed that the basal channel section along the 2020 fracture line was near a state of neutral mass balance from July 2015 to July 2019, with around 1 m of ice melting in summer, and compensating frazil ice accretion in winter [13]. Using the fact that velocities and temperature scale linearly with ice melting [24], basal melting in the channel was ~40% higher (1.4 m) for the period of July 2019 to July 2020 before the breakup (methods). This additional melting is not enough to have completely melted

ARTICLE IN PRESS

the channel roof. Moreover, the fact that Ice Island A and B broke apart along the basal channel only after the calving (Figure 3b) suggests melting in the basal channel did not trigger the calving. Its collapse between the disintegrated region and Ice Island A may have allowed fracture propagation from NE to SW, or vice versa.

Following the calving event, the epishelf lake water continued to warm until the end of August and reached 4ºC, the highest since monitoring began (Figure 5a). The warm epishelf lake water flowing through the remaining basal channel likely melted the roof enough to lead to its collapse sometime in the year after calving (Figure 6b).

e. Loss of sea ice buttress

The northern coast of Ellesmere Island has historically been characterized by a fringe of perennial sea ice, which acts as a buttress for ice shelves and provides protection from ocean swell. The loss of sea ice along this coast has been identified as an important factor in previous calving events [25], similar to Antarctica [e.g. 22]. In both 2019 and 2020, the number of days the ice shelf was exposed to open ocean (or mobile ice) was above the 2001-2020 average (Figure 5e,f), possibly leading to enhanced flexural stresses and fracturing from ocean swell [21,22] and reducing the buttressing potential that may have previously stabilized the ice shelf [22,26,27].

In early July 2020, a vast area of open water was persistent along the northern coast of Ellesmere Island. On July 14 2020 a 5-10 km wide section of land-fast sea ice attached to the MIS broke free, exposing the eastern seaward edge of the MIS directly to open ocean for two weeks prior to the calving. Moderate winds (4.12 m s^{-1} average ±1.87 m s^{-1}) possibly generated swell from the 15th to the 22nd before moving ice appeared with lower winds (average 3.64 m s^{-1} ±2.08 m s^{-1}) from the 23th to the 31th (Figure S1).

Remote sensing imagery did not reveal new visible fractures or ridges in 2019 or in 2020 before the calving. However, it is possible that fractures below the resolution of the imagery existed prior to the event and that the lack of sea ice simply allowed the ice shelf pieces to drift apart. In addition, a patch of multiyear landfast sea ice was still attached to the western edge of the ice shelf when calving occurred (Figure 3b). The low winds, the presence of mobile sea ice and the absence of new visible weaknesses during open ocean conditions suggest ocean swell did not directly trigger the calving event. Nonetheless, calving would likely not occur with sea ice protecting the MIS, highlighting the importance of sea-ice conditions adjacent to the ice shelf.

f. Hydrofracture

Elevated surface melt during summer 2019 and 2020 also increased the volume of surface meltwater ponds, which are prominent features of MIS (Figure 2). The western portion of the ice shelf disintegrated where large surface meltwater ponds were present the day before calving (Figure 3e), in a similar fashion to other calving event induced by hydrodracture [23,28]. Hydrofracture needs an existing crevasse to initiate. This starting point could be the relatively young fracture near one of the largest meltwater pond along which the western section subsequently fractured (Figure 3f). With ice thicknesses of approximately 48 m and meltwater ponds level reaching within a few meters of the surface, only modest tensile stresses (25-50 kPa) and shallow pre-existing crevasses (3-25 m) are required for hydrofracture to propagate through the full ice thickness (methods, Figure S2). Such conditions would favor a chain reaction whereby hydrofracture of one ponded region destabilizes adjacent regions of similar thickness and meltwater level, leading to progressive disintegration of neighboring portions of the ice shelf [23].

g. Sequence of ice shelf calving and epishelf lake drainage

Our analysis indicates that the cumulation of the long-term negative surface and basal mass balance (combined thinning of 0.26 m w.e.a^{-1} over the calved section), along with pre-existing structural

ARTICLE IN PRESS

weaknesses put the ice shelf in an increasingly vulnerable state over the past decades. In the weeks prior to calving, open ocean conditions with moderate winds and higher than normal basal melting along the basal channel likely contributed to the calving. However, the disintegration of the NW section of the ice shelf and the presence of large meltwater ponds in the proximity of a relatively new fracture suggests hydrofracture may have triggered the breakup.

The loss of the ice dam located on the outer portion of the ice shelf allowed the release of epishelf lake freshwater to the ocean. The elevated water temperature and presumably high flow during the drainage of lake waters likely further promoted enhanced submarine melting of the channel roof, resulting in its eventual collapse (Figures 3d and 6b) and the complete loss of the epishelf lake. The remaining sections of the MIS are thinner and more fractured than the section that calved away, leaving it vulnerable to further collapse.

5. Epishelf Lakes as Sentinel Ecosystems

Epishelf lakes are tightly coupled to the state of the impounding ice shelf, and changes in the lake ecosystem can act as a sentinel, signaling a change in the ice shelf or surrounding cryosphere[7]. For example, the Disraeli Fiord epishelf lake shoaled substantially in the decade prior to the collapse of the Ward Hunt Ice Shelf [7]. Water level data from Beaver Lake in East Antarctica were used to infer that the neighboring Amery Ice Shelf was becoming thicker [29]. Water profiles in epishelf lake Blåsø allowed the detection of warm Atlantic water close to the grounding line of 79N Glacier in Greenland which could lead to enhanced melting of the impounding glacier tongue [30]. The salinity increase in Milne Fiord epishelf lake since 2018 suggests a fundamental shift in the integrity of the MIS was underway, culminating in the calving event. Epishelf lakes provide a valuable source of information about the health of their ice shelves and associated ecosystems, and those remaining in Greenland and Antarctica require close monitoring.

Previous studies on Milne Fiord epishelf lake ecosystem prior to the ice shelf calving showed that it contained many planktonic taxa that are typical of Arctic freshwater lakes, including the copepod *Limnocalanus macrurus*, phototrophic picocyanobacteria and heterotrophic *Polaromonas* [3,31]. Salinity is a major ecological filter on plankton composition, including in coastal high latitude waters [32], and it is therefore likely that the largescale shift from freshwater to saltwater in the Milne Fiord ecosystem (Figure 4a) resulted in a complete reconfiguration of the zooplankton, phytoplankton and bacterioplankton communities in its upper waters, with associated effects on food web and biogeochemical processes.

6. Outlook

The collapse of the Milne Ice Shelf and resulting loss of the last epishelf lake along the northern coast of Ellesmere Island marks a regime shift and the end of a 4000-year era. Milne Fiord is now in the process of transforming from a perennially ice-covered fjord protected by an ice shelf to a seasonally ice-free fiord, as has already occurred in every other glacial fjord along this coast [3]. Fjords in northern Greenland are also experiencing a similar transformation, with rapid attrition of their ice shelves [33-35].

Milne Fiord is located at the center of the Last Ice Area and the Tuvaijuittuq Marine Protected Area (MPA). Known in Inuktitut as “the place where the ice never melts”, it is the region projected to maintain the last perennial sea ice in the northern hemisphere. Fjords and ice shelves are ecologically significant components of this MPA [36]. Our reporting of the breakup of Milne Ice Shelf and drainage of the last epishelf lake in Canada shows that high latitude ecosystems are changing rapidly, even in this region considered as the ultimate Arctic refuge. While ecosystems at lower latitudes may migrate poleward in response to warming [37], ice-dependent systems at the climatic limit of the Arctic have no further refuge. The disappearance of epishelf lakes in

ARTICLE IN PRESS

Canada thus represents the loss of unique high-Arctic ecosystems. Their re-establishment would require ice shelves to recover, which is not possible given the current climate trajectory.

Methods

a. Ocean observations

From May 2011 to July 2024, annual Conductivity-Temperature-Depth (CTD) profiles were collected at the mooring location and offshore (except in 2020 and 2021). Conductivity was converted to absolute salinity (S_A) using the TEOS-10 oceanographic toolbox [38]. A mooring was installed near the center of the epishelf lake in May 2011 through a hole cut with an ice saw in the ~2 m thick epishelf lake ice. The mooring has recorded oceanographic conditions since that time. The instruments in the upper 50 m were employed to analyse the evolution of the epishelf lake and the possible influence of ocean temperature on ice shelf calving. The configuration of the mooring is described in supplementary information. Linear interpolation between loggers was used to determine the temperature at 5 and 45 m when the loggers were not exactly at these depths. The maximum distance between a logger and the 5 and 45 m depths was 1.2 and 5.0 m, respectively. Comparison to the CTD profiles from 2011 to 2020 indicates mean (max) errors of 0.14 (0.40) and 0.07 (0.24) ˚C for the 5 and 45 m interpolated values, respectively.

To estimate the melting increase in the basal channel for the July 2019-July 2020 period, the linear response of melting to water velocity and temperature was used. The negative surface mass balance was used as a proxy for velocity as water entering the epishelf lake from surface melt must exit through the basal channel; more surface inflow equates to faster basal channel outflow. Since velocity times temperature is proportional to the melting rate [24], the sum of the negative surface mass balance times the water temperature at 5 m depth was used to estimate the annual relative basal channel melting. From July 2015 to 2019, the yearly average of this quantity was -0.54 m w.e.a^{-1} ºC. For the July 31 2019 to July 31 2020 period, it was -0.76 m w.e.a^{-1} ºC , 40% higher.

For consistency with previous studies on Milne Fiord epishelf lake [10,11], the depth of the bottom of the lake was defined as the depth where the density gradient is the largest, measured using the buoyancy frequency, $N^2 = -g\rho_o^{-1}\partial\rho/\partial z$. Where z is positive upwards, ρ is density and ρ_o is a reference density, here 1023 g kg^{-1} (average between freshwater and seawater). Considering a lowering speed of <0.5 m s^{-1} and an instrument sampling frequency of >6 Hz, the uncertainty of the epishelf lake depth from CTD profiles is <0.08 m.

To estimate the lake depth from the mooring data, the closest in time CTD profile was fitted to the salinity instruments on the mooring by moving it vertically to minimize the root mean squared error between the profile and the instruments measurements. The CTD profiles since 2011 show that the transition between 1 g kg^{-1} and 22 g kg^{-1} was always between 2.2 and 4.2 m thick. Since the depth of the epishelf lake was only estimated when a mooring instrument measured a salinity between 1 and 22 g kg^{-1}, the uncertainty of the mooring-derived epishelf lake is 2.0 m. Except in 2012 when a mixing event broadened the bottom of the halocline. For that year, the uncertainty is higher, but the instruments shallower than 7 m depth confirm the lake was deeper than 7 m.

To investigate the influence of sea ice on calving, MODIS imagery from 2001 to 2020 was employed to calculate the number of days with at least 10 km free of ice in front of the MIS and to calculate the number of days with mobile ice (not fast). These ice-free and mobile ice calculations were performed manually using daily image mosaics.

b. Atmospheric and glaciological observations

To assess the influence of surface mass balance on the calving event, we used the surface mass balance estimates from RACMO2.3 [39]. The negative surface mass balance estimates of the two glaciers on each side of MIS at the first grid cell above sea level was used. The average of the two

ARTICLE IN PRESS

was used and a factor of 0.2 was applied to match the observed surface ablation on the MIS (-0.30 m w.e. a^{-1} [16]).

To examine structural weaknesses in the MIS, the 2 m resolution ArcticDEM elevation mosaic [15] constructed with images from 2008 to 2018 was used to estimate ice thickness (Figure 2a). The DEM was referenced to sea level by using the elevation of the epishelf lake ice cover as a datum (0.2 m above sea level). Hydrostatic equilibrium was then used assuming an MIS ice density of 900 kg m^{-3} [40,41] and a fjord water density of 1023 kg m^{-3}. Using these density values gives the exact ice thickness along a 4 km-long ice penetrating radar survey from 2019 (Figure S3). Since the ArcticDEM data is from 2008 to 2018, the thickness may vary depending on the acquisition date and ice shelf thinning. We evaluate the uncertainty of our thickness estimates to be plus/minus 11 years of thinning (±2.9 m).

The timing and evolution of the calving event was investigated using Sentinel-1, Sentinel-2 and Planet Lab imagery at 1:25,000 scale in QGIS (version 3.34) using the Albers projection and methods described in Mueller et al. [42]. The pre-calving extent of the MIS was determined by updating a 187.4 km² polygon digitized from a Fine Quad Radarsat-2 image [42] with a Planet image from July 26, 2020. The northern edge of the ice shelf post-calving was delineated using Sentinel-2 and Planet imagery from July 31 and verified against a Planet image from August 11. The two largest ice islands (A and B in Figure 3b, but following further deterioration) were delineated in an August 4 and 5 Sentinel-1 image, respectively. To determine the thickness of the ice islands, each polygon was rotated and translated back to its pre-calving origin and the DEM was clipped to determine the mean thickness via hydrostatic equilibrium in these areas. Uncertainty in digitization was determined using the methods in Mueller et al. [42] based on the resolution of the imagery used for digitization, modified by an empirical factor and offset to account for repeatability. Ice type identification can be error-prone, and it should be noted that the southern third of the MIS is undergoing rapid melting and breakup in situ and it is not possible with this technique to fully distinguish between ice shelf and independent fragments.

For context on the atmospheric forcing of surface mass balance, we use observations from Alert (270 km west) from 1953 to present to evaluate the effect of air temperature. This is done by calculating the cumulative amount of degree-day above zero for each year.

c. Hydrofracture criterion

The potential for meltwater-driven hydrofracture was evaluated using linear elastic fracture mechanics following Van der Veen [43]. The stress intensity factor at the tip of a water-filled crevasse was expressed as the sum of contributions from far-field tensile stress, ice overburden pressure, and water pressure,

$$K_I = K_R + K_i + K_w,$$

where

$$K_R = F(\gamma) R_{xx} \sqrt{\pi d},$$

$$K_i = \frac{2\rho_i g}{\sqrt{\pi d}} \int_0^d \left[-b + \frac{\rho_i - \rho_s}{\rho_i C} (1 - e^{-Cb}) \right] G(\gamma,\lambda) db$$

and

$$K_w = \frac{2\rho_w g}{\sqrt{\pi d}} \int_0^d (b - a) G(\gamma,\lambda) db\,.$$

Here, R_{xx} is the far-field tensile stress, d is the crevasse depth, H is the ice thickness, a is the depth of the water surface below the ice surface, g is the gravitational acceleration. ρ_i, ρ_s and ρ_w are the

ARTICLE IN PRESS

ice density at depth (900 kg m^3), near the surface (860 kg m^3) and freshwater density (1000 kg m^3). $F(\gamma)$ and $G(\lambda,\gamma)$ are geometrical functions with $\gamma = d/H$ and $\lambda = b/d$. C is an exponent to describe the ice density increase from the surface to depth taken as 0.05 here to follow the density profiles from an Arctic Ice Island [40]. Fracture propagation occurs when the stress intensity factor exceeds the fracture toughness of ice,

$$K_I \geq K_{Ic},$$

where K_{Ic} generally lies between 100 and 400 kPa m$^{1/2}$ [43]. For the western portion of the Milne Ice Shelf, characteristic ice thickness was taken to be 48 m and meltwater ponds were assumed to maintain water levels within 3 m of the ice surface. Because hydrofracture initiates from pre-existing crevasses, the relevant criterion is that K_I exceeds K_{Ic} throughout the propagation pathway from an initial crevasse depth d_0 to the ice base. Under these conditions, pre-existing crevasses 5–10 m deep require tensile stresses of approximately 50 kPa to propagate through the full ice thickness, while deeper crevasses of 15–20 m require stresses smaller than 25 kPa. These values of tensile stress are on the lower end of what is usually expected to cause crevasse deepening and fracture propagation for a single fracture [43-45].

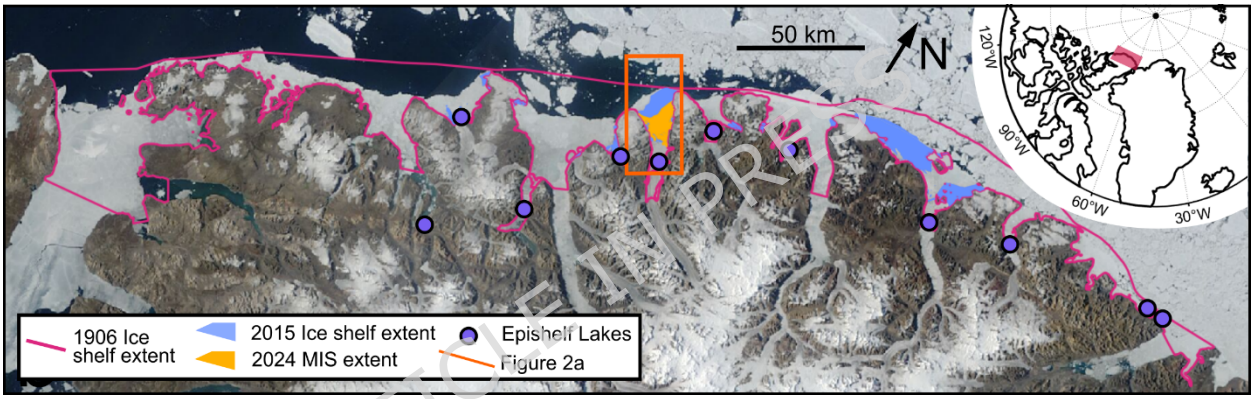


Figure 1. Northern Coast of Ellesmere Island on July 21, 2020. MODIS image retrieved from NASA Worldview (https://worldview.earthdata.nasa.gov/) showing the dramatic decrease in ice shelf extent since 1906 and the location of now vanished epishelf lakes [3,42]. The top right inset shows the location of image.

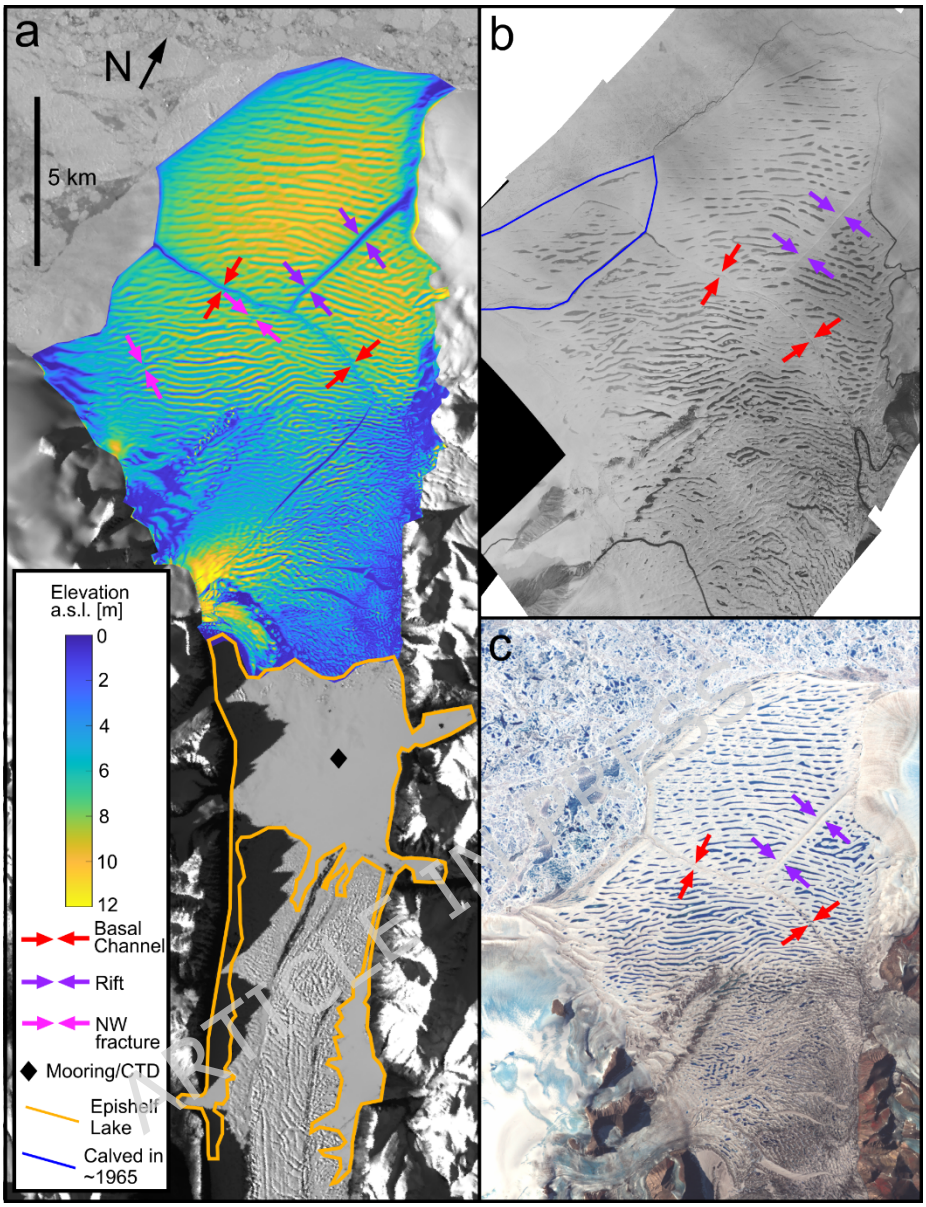


Figure 2. Milne Ice Shelf and Milne Fiord epishelf lake. a) Landsat-8 image of Milne Fiord from September 2018 (retrieved from https://earthexplorer.usgs.gov/ USGS EarthExplorer) with Milne Ice Shelf ice surface elevation from ArcticDEM mosaic (retrieved from https://arcticdem.apps.pgc.umn.edu/) and the Milne Fiord epishelf lake (MEL) outline. b) 1959 aerial mosaic image of Milne Ice Shelf (CC-BY; Government of Canada) with the area that calved around 1965 [46]. c) July 2009 ASTER image of Milne Ice Shelf (retrieved from NASA Earthdata (https://search.earthdata.nasa.gov/).

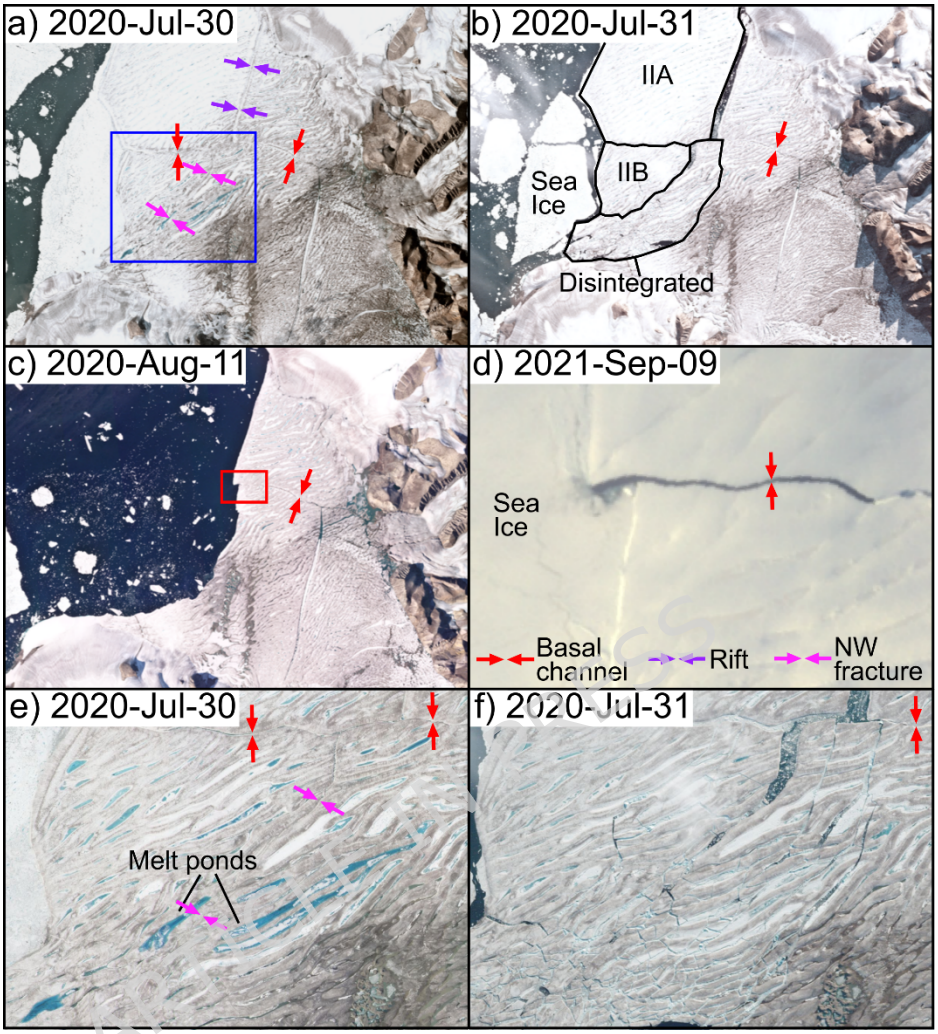


Figure 3. Satellite images of the Milne Ice Shelf calving event. a) Pre-calving, the blue box shows the extent of panels e)-f). b) During calving with Ice Island A (IIA), Ice Island B (IIB), and the region where the ice shelf disintegrated into smaller fragments. c) Post-calving, the red box shows the extent of panel d). d) Zoom-in of a section of the basal channel post-calving, where the roof has collapsed and open water is visible in the channel. e) Zoom-in of the disintegrated section showing the large melt ponds. f) Zoom-in of the disintegrated section showing the multiple fractures along and across the ice shelf rolls. Panels a,b,c,e ad f are PlanetScope images downloaded from the from Planet Explorer and panel d is a Sentinel 2 image downloaded from Copernicus Browser (https://browser.dataspace.copernicus.eu/.

ARTICLE IN PRESS

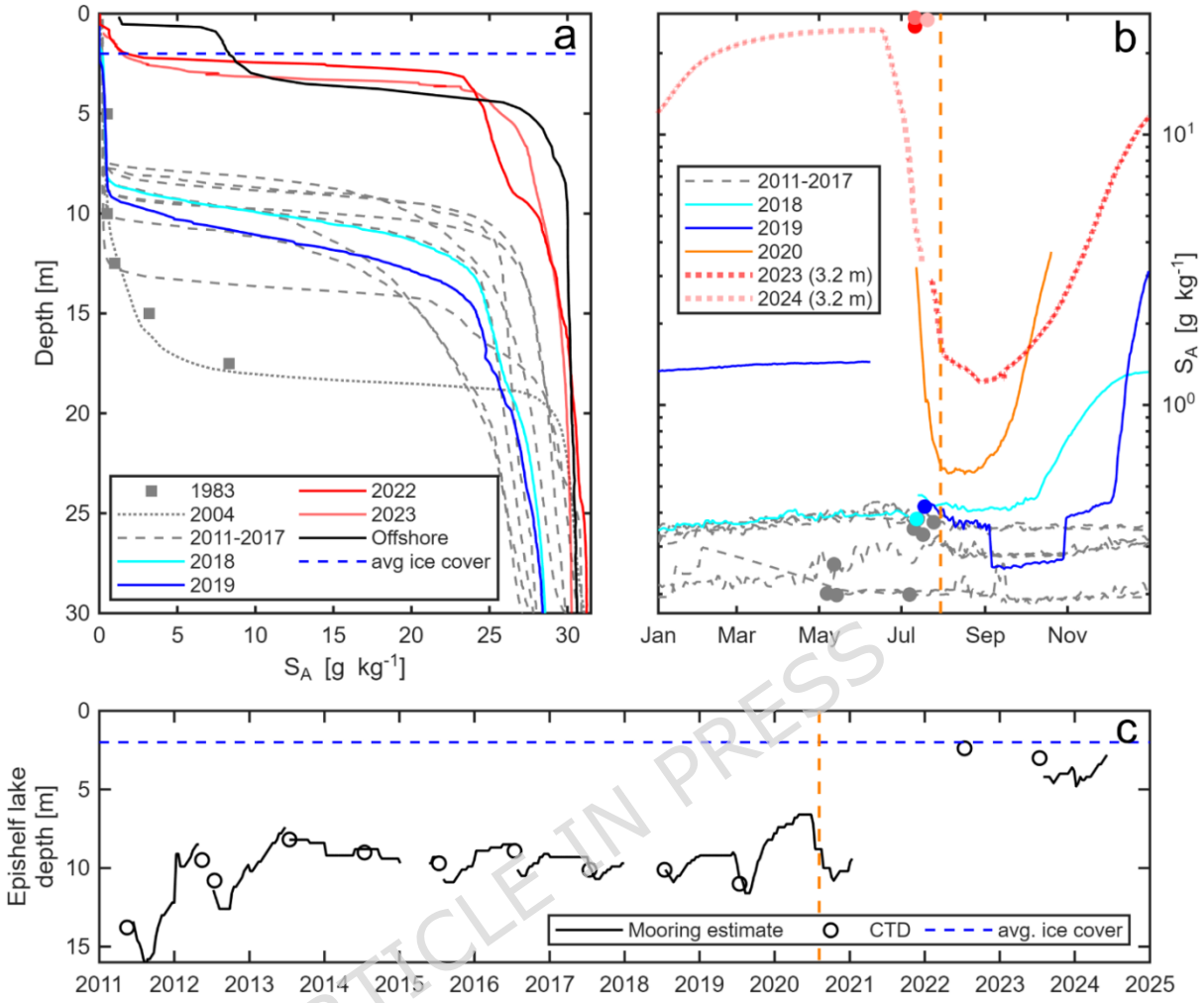


Figure 4. Milne Fiord Epishelf Lake drainage. a) Upper water column profiles showing the contraction of the epishelf lake following the MIS calving event. Salinity is now above 1 g kg^{-1} just under the ice. b) Time series of salinity at 6.2 (2011-2020) and 3.2 (2023-2024) m depth. The dots are salinity measurements at 6.2 m from CTD profiles over 2023 and 2024. Freshwater (<1 g kg^{-1}) was present down to at least 6.2 m depth before 2017. After a slight salinity increase in winter of 2018 and 2019, perhaps indicating the ice shelf integrity was compromised, there was an increase to seawater salinity all year after the calving event. c) Time series of epishelf lake depth (maximum stratification) from CTD and estimated from mooring data (see methods). The vertical dashed line in b) and c) show the timing of the calving event.

ARTICLE IN PRESS

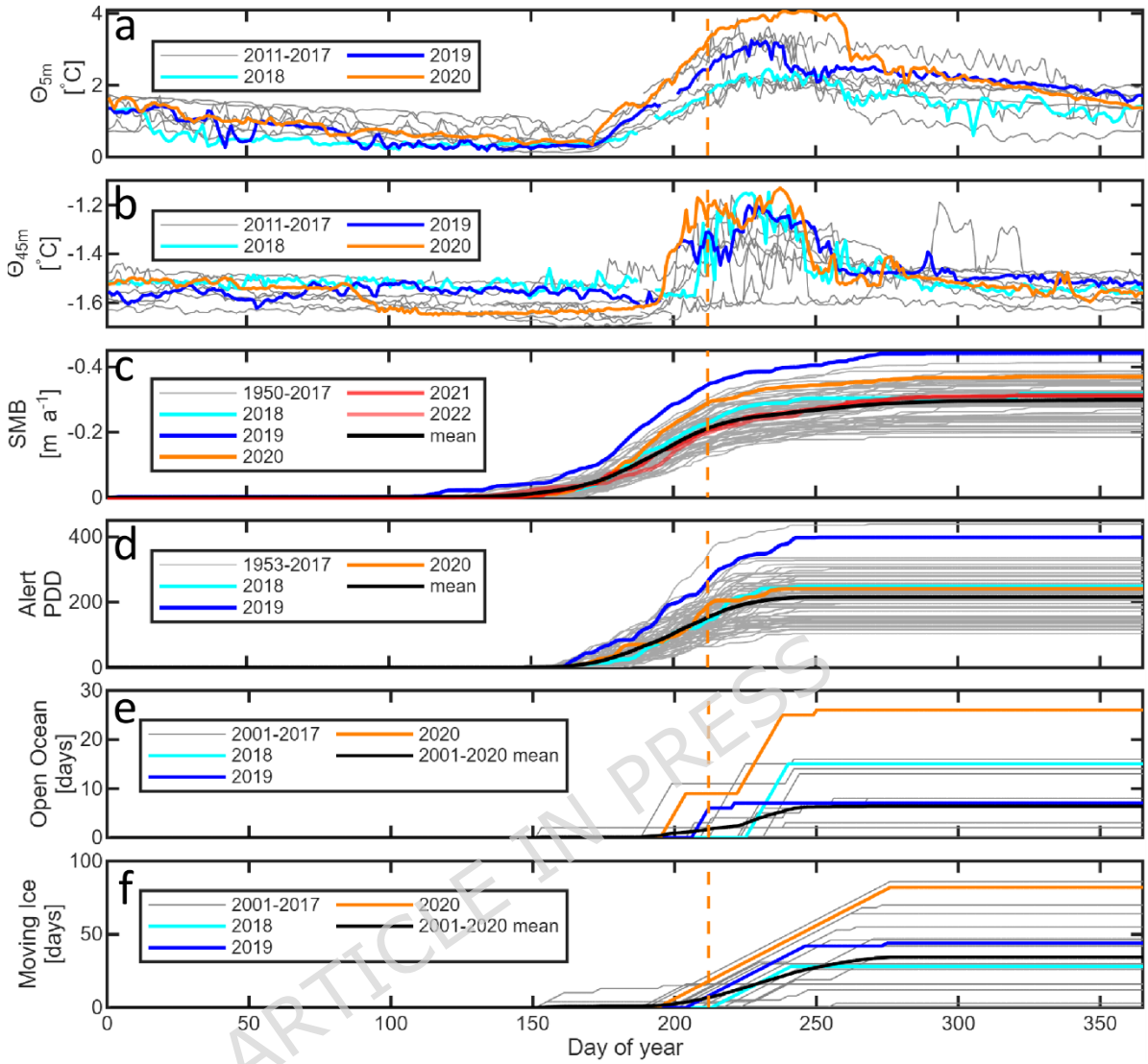


Figure 5. Observations related to the MIS calving event. a) Water temperature at 5 m depth in the epishelf lake. b) Ocean temperature at 45 m depth (average MIS thickness). c) MIS surface mass balance. d) Cumulative Positive Degree Days (PDD) in Alert (275 km to the east). e) Cumulative number of days with open ocean in front of MIS. f) Cumulative number of days with mobile ice in front of MIS. The vertical line on day 212 denotes the day of the calving event.

ARTICLE IN PRESS

ARTICLE IN PRESS

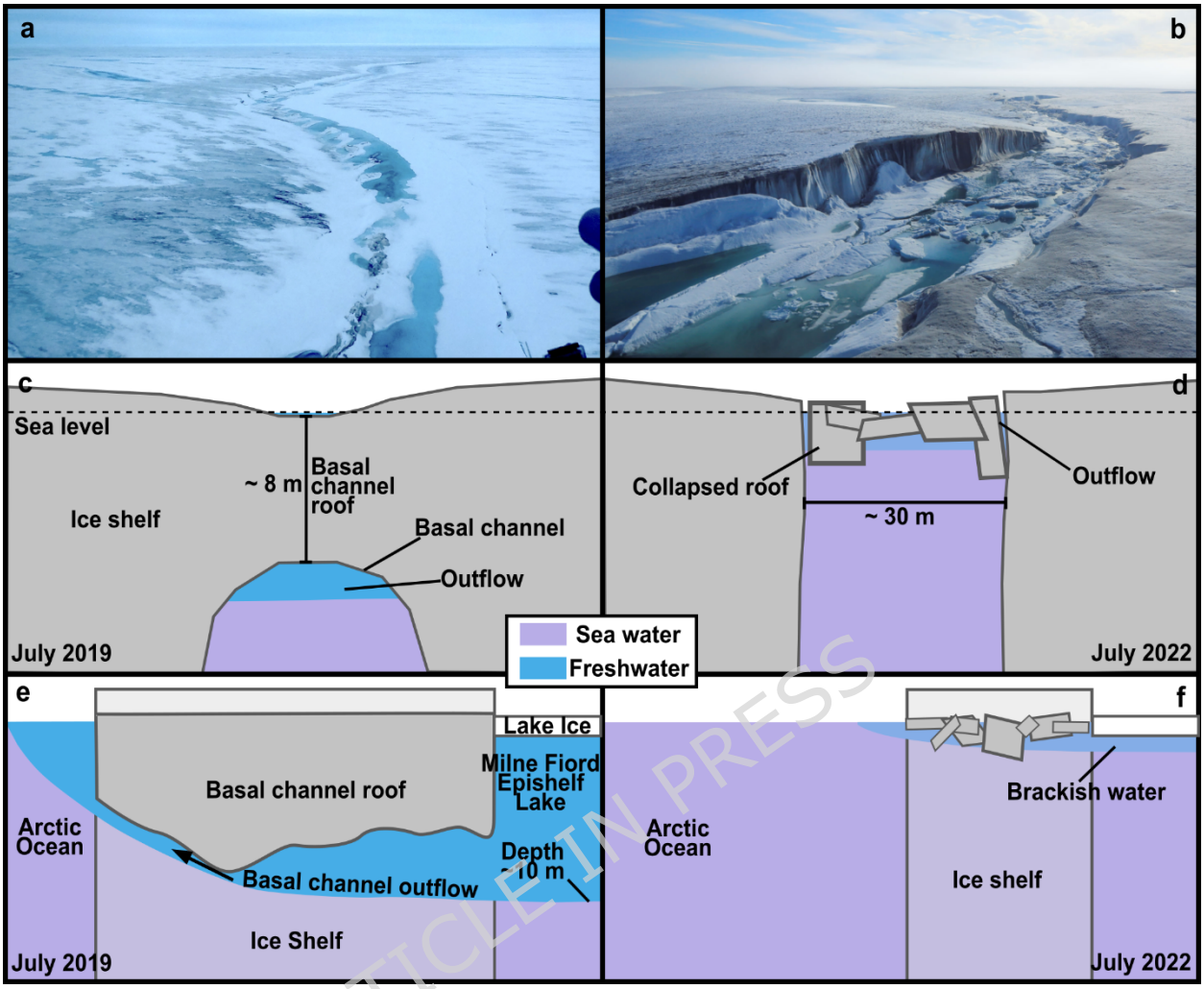


Figure 6. Connection between the Milne Fiord epishelf lake and the ocean. a) Photo of the basal channel before the calving event (July 2019; photo credit: Derek Mueller). b) Photo of the basal channel after the calving event (July 2023; CC BY, photo credit: Cameron Fitzpatrick). Schematics of cross-sections across the basal channel before (c) and after (d) the calving event. Schematics of cross-sections along the basal channel before (e) and after (f) the calving event. In panel e, the darker ice polygon is the ice shape along the basal channel and the lighter ice rectangle is the ice shape behind (thicker with more freeboard).

Acknowledgements

The authors are thankful for the logistical support given by the Polar Continental Shelf Program and would like to thank all the individuals who took part in field campaigns in Milne Fiord over the years. We also acknowledge B. Noël for providing the RACMO2.3 data.

Funding

This project was supported by the following organizations: Killam Foundation, The University of British Columbia, Natural Sciences and Engineering Research Council of Canada, The Polar Continental Shelf Program, ArcticNet, Canada Foundation for Innovation, The Ontario Research Foundation Polar Knowledge Canada, Polar Knowledge Canada, the Trebek Initiative, the Weston Foundation, the Royal Society and the Royal Society of Edinburgh.

Data availability

ARTICLE IN PRESS

The water profiles and the mooring data are freely available on the Polar Data Catalogue [47-49] (https://polardata.ca/).

References

1. Vincent, W. F., & Mueller, D. Witnessing ice habitat collapse in the Arctic. *Science 370*(6520), 1031-1032 (2020).
2. Girard, C., Culley, A.I, and Vincent, W.F. Arctic bacterial diversity and connectivity in the coastal margin of the Last Ice Area. *ISME Communications* 3:105. doi:10.1038/s43705-023-00313-w (2023).
3. Veillette, J., Mueller, D. R., Antoniades, D., & Vincent, W. F. Arctic epishelf lakes as sentinel ecosystems: Past, present and future. *Journal of Geophysical Research: Biogeosciences* 113(G4) (2008)
4. Heywood, R. B. A limnological survey of the Ablation Point area, Alexander Island, Antarctica. *Philosophical Transactions of the Royal Society of London. B, Biological Sciences* 279(963), 39-54 (1977).
5. Laybourn-Parry, J., Quayle, W. C., Henshaw, T., Ruddell, A., & Marchant, H. J. Life on the edge: the plankton and chemistry of Beaver Lake, an ultra-oligotrophic epishelf lake, Antarctica. *Freshwater Biology* 46(9), 1205-1217. (2001).
6. Van Hove, P., Swadling, K. M., Gibson, J. A., Belzile, C., & Vincent, W. F. Farthest north lake and fjord populations of calanoid copepods *Limnocalanus macrurus* and *Drepanopus bungei* in the Canadian high Arctic. *Polar Biology* 24(5), 303-307 (2001).
7. Mueller, D. R., Vincent, W. F., & Jeffries, M. O. Break-up of the largest Arctic ice shelf and associated loss of an epishelf lake. *Geophysical Research Letters* 30(20) (2003).
8. Antoniades, D., Francus, P., Pienitz, R., St-Onge, G., Vincent, W.F. Holocene dynamics of the Arctic's largest ice shelf. *Proceedings of the National Academy of Science* 108(47), 18899-18904 (2011).
9. Labbé, M., Thaler, M., Pitot, T. M., Rapp, J. Z., Vincent, W. F., & Culley, A. I. Climate-endangered Arctic epishelf lake harbors viral assemblages with distinct genetic repertoires. *Applied and Environmental Microbiology* 88(17), e00228-22 (2022).
10. Hamilton, A. K., Laval, B. E., Mueller, D. R., Vincent, W. F., & Copland, L. Dynamic response of an Arctic epishelf lake to seasonal and long-term forcing: implications for ice shelf thickness. *The Cryosphere*, 11(5), 2189-2211 (2017).
11. Bonneau, J., Laval, B. E., Mueller, D., Hamilton, A. K., Friedrichs, A. M., & Forrest, A. L. Winter dynamics in an epishelf lake: Quantitative mixing estimates and ice shelf basal channel considerations. *Journal of Geophysical Research: Oceans*, 126(9), e2021JC017324 (2021).
12. Rajewicz, J. S. *Channelized epishelf lake drainage beneath the Milne Ice Shelf, Ellesmere Island, Nunavut* (Master's thesis, Carleton University) (2017).
13. Bonneau, J., Rajewicz, J. S., Friedrichs, D. M., Mueller, D., Laval, B. E., Forrest, A. L., ... & Steiner, O. S. Momentum, Heat, and Salt Budgets to Estimate Drag and Transfer Coefficients inside an Ice Shelf Basal Channel. *Journal of Physical Oceanography* 55(9), 1353-1373 (2025).
14. Jeffries, M. O. Physical, chemical and isotopic investigations of Ward Hunt Ice Shelf and Milne Ice Shelf, Ellesmere Island, NWT. (Doctoral dissertation, University of Calgary) (1985).
15. Porter, C., Morin, P., Howat, I., Noh, M.-J., Bates, B., Peterman, K., et al. ArcticDEM. Harvard Dataverse, 1, 2018–2030. (2018).

ARTICLE IN PRESS

16. Mortimer, C. A., Copland, L., & Mueller, D. R. Volume and area changes of the Milne Ice Shelf, Ellesmere Island, Nunavut, Canada, since 1950. *Journal of Geophysical Research: Earth Surface* 117(F4) (2012).
17. White, A. *Glacier changes across Northern Ellesmere Island* (Doctoral dissertation, Université d'Ottawa/University of Ottawa) (2019).
18. Bonneau, J., Laval, B. E., Mueller, D., Antropova, Y., & Hamilton, A. K. The impact of ice structures and ocean warming in Milne Fiord. *The Cryosphere*, 19(7), 2615-2633 (2025).
19. Bassis, J. N., Crawford, A., Kachuck, S. B., Benn, D. I., Walker, C., Millstein, J., ... & Luckman, A. Stability of ice shelves and ice cliffs in a changing climate. *Annual Review of Earth and Planetary Sciences*, *52*(1), 221-247 (2024).
20. Benn, D. I., Luckman, A., Åström, J. A., Crawford, A. J., Cornford, S. L., Bevan, S. L., ... & Bassis, J. Rapid fragmentation of thwaites eastern ice shelf. *The Cryosphere*, *16*(6), 2545-2564 (2022).
21. Teder, N. J., Bennetts, L. G., Reid, P. A., Massom, R. A., Pitt, J. P., Scambos, T. A., & Fraser, A. D. Large-scale ice-shelf calving events follow prolonged amplifications in flexure. *Nature Geoscience*, *18*(7), 599-606 (2025).
22. Massom, R. A., Scambos, T. A., Bennetts, L. G., Reid, P., Squire, V. A., & Stammerjohn, S. E. Antarctic ice shelf disintegration triggered by sea ice loss and ocean swell. *Nature* 558(7710), 383-389 (2018).
23. Banwell, A. F., MacAyeal, D. R., & Sergienko, O. V. Breakup of the Larsen B Ice Shelf triggered by chain reaction drainage of supraglacial lakes. *Geophysical Research Letters* 40(22), 5872-5876 (2013).
24. Holland, D. M., & Jenkins, A. (1999). Modeling thermodynamic ice–ocean interactions at the base of an ice shelf. *Journal of Physical Oceanography*, *29*(8), 1787-1800.
25. Copland, L., Mortimer, C., White, A., Richer McCallum, M., & Mueller, D. Factors contributing to recent Arctic ice shelf losses. In *Arctic ice shelves and ice islands* (pp. 263-285). Dordrecht: Springer Netherlands (2017).
26. Massom, R. A., Giles, A. B., Warner, R. C., Fricker, H. A., Legresy, B., Hyland, G., ... & Young, N. External influences on the Mertz Glacier Tongue (East Antarctica) in the decade leading up to its calving in 2010. *Journal of Geophysical Research: Earth Surface*, *120*(3), 490-506 (2015).
27. Arthur, J. F., Stokes, C. R., Jamieson, S. S., Miles, B. W., Carr, J. R., & Leeson, A. A. (2021). The triggers of the disaggregation of Voyeykov Ice Shelf, Wilkes Land, East Antarctica, and its subsequent evolution. *Journal of Glaciology*, *67*(265), 933-951 (2021).
28. Scambos, T. A., Hulbe, C., Fahnestock, M., & Bohlander, J. The link between climate warming and break-up of ice shelves in the Antarctic Peninsula. *Journal of Glaciology* 46(154), 516-530 (2000).
29. Galton-Fenzi, B. K., Hunter, J. R., Coleman, R., Marsland, S. J., & Warner, R. C. Modeling the basal melting and marine ice accretion of the Amery Ice Shelf. *Journal of Geophysical Research: Oceans* 117(C9) (2012).
30. Bentley, M. J., Smith, J. A., Jamieson, S. S., Lindeman, M. R., Rea, B. R., Humbert, A., ... & Roberts, D. H. Direct measurement of warm Atlantic Intermediate Water close to the grounding line of Nioghalvfjerdsfjorden (79°N) Glacier, northeast Greenland. *The Cryosphere* 17(5), 1821-1837 (2022).

ARTICLE IN PRESS

ARTICLE IN PRESS

31. Thaler, M., Vincent, W. F., Lionard, M., Hamilton, A. K., & Lovejoy, C. Microbial community structure and interannual change in the last epishelf lake ecosystem in the north polar region. *Frontiers in Marine Science,* 3, 275 (2017).
32. Blais, M. A., Matveev, A., Lovejoy, C., & Vincent, W. F. Size-fractionated microbiome structure in subarctic rivers and a coastal plume across DOC and salinity gradients. *Frontiers in Microbiology*, 12, 760282 (2022).
33. Hill, E. A., Carr, J. R., & Stokes, C. R. A review of recent changes in major marine-terminating outlet glaciers in Northern Greenland. *Frontiers in Earth Science* 4, 111 (2017).
34. Millan, R., Jager, E., Mouginot, J., Wood, M. H., Larsen, S. H., Mathiot, P., ... & Bjørk, A. Rapid disintegration and weakening of ice shelves in North Greenland. *Nature Communications* 14(1), 6914 (2023).
35. Ochwat, N., Scambos, T., Fahnestock, M., & Stammerjohn, S. (2023). Characteristics, recent evolution, and ongoing retreat of Hunt Fjord Ice Shelf, northern Greenland. *Journal of Glaciology*, *69*(273), 57-70.
36. DFO. Identification of Ecological Significance, Knowledge Gaps and Conservation Objectives for the Tuvaijuittuq Marine Protected Area. *DFO Can. Sci. Advis. Sec. Sci.* Resp. 2020/056 (2020)
37. Chen, I. C., Hill, J. K., Ohlemüller, R., Roy, D. B., & Thomas, C. D. Rapid range shifts of species associated with high levels of climate warming. *Science* 333(6045), 1024-1026 (2011).
38. McDougall, T. J. & Barker, P. M. Getting started with TEOS-10 and the Gibbs Seawater (GSW) Oceanographic Toolbox, 28pp., SCOR/IAPSO WG127, ISBN 978-0-646-55621-5 (2011).
39. Noël, B., Van De Berg, W. J., Van Wessem, J. M., Van Meijgaard, E., Van As, D., Lenaerts, J., ... & Van Den Broeke, M. R. Modelling the climate and surface mass balance of polar ice sheets using RACMO2–Part 1: Greenland (1958–2016). *The Cryosphere* 12(3), 811-831 (2018).
40. Poplin, J. P., & Ralston, T. D. Physical and mechanical properties of Hobson's Choice Ice Island cores. *Cold regions science and technology*, *20*(2), 207-223 (1992).
41. Jeffries, M. O. *Physical, chemical and isotopic investigations of ward Hunt ice shelf and Milne ice shelf, Ellesmere Island*, *NWT*. (Doctoral Dissertation, University of Calgary) (1985).
42. Mueller, D., Copland, L. & Jeffries, M. O. Changes in Canadian Arctic ice shelf extent since 1906. in *Arctic Ice Shelves and Ice Islands* (eds Copland, L. & Mueller, D.) 109–148. Springer, Dordrecht. (2017).
43. Van der Veen, C. J. Fracture mechanics approach to penetration of surface crevasses on glaciers. *Cold Regions Science and Technology*, *27*(1), 31-47 (1998).
44. Marsh, O. J., Arthern, R. J., & De Rydt, J. Ocean tides trigger ice shelf rift growth and calving. *Nature Communications*, *16*(1), 6697 (2025).
45. Vaughan, D. G. Relating the occurrence of crevasses to surface strain rates. *Journal of Glaciology*, *39*(132), 255-266 (1993).
46. Jeffries, M. O. The growth, structure and disintegration of Arctic ice shelves. *Polar Record*, *23*(147), 631-649. (1987).
47. Mueller, D., Hamilton, A. K., Bonneau, J., Friedrichs, D. M., Rajewicz, J. S., White, A., Copland, L., Garbo, A., Richer McCallum, M., Antropova, Y., Crocker, G., de Jong, T.,

ARTICLE IN PRESS

Graves, K., Kim, J., Brenner, S., Wilson, N., Wray, P., Xu, K., Mortimer, C., Pope, S., Forrest, A., and Laval, B. E.: Milne Fiord CTD (Conductivity, Temperature, Depth) profiles, 2008–2019, Polar Data Catalogue [data set], https://doi.org/10.21963/12102, (2021)

48. Mueller, D., Hamilton, A. K., Bonneau, J., and Laval, B. E.: Milne Fiord Oceanographic Mooring, 2011–2019, Polar Data Catalogue [data set], https://doi.org/10.21963/12101, (2021).
49. Mueller, D., Bonneau, J., Hamilton, A. K., Antropova, Y., Forrest, A. L., and Laval, B. E.: Milne Fiord CTD (Conductivity, Temperature, Depth) profiles, Polar Data Catalogue [data set], https://doi.org/10.21963/13383 (2024)
50. Hersbach, H., Cobb, A., Kaandrop, M., Poli, P., Bell, B., Berrisford, P., Biavati, G., Horányi, A., Muñoz Sabater, J., Nicolas, J., Peubey, C., Radu, R., Rozum, I., Schepers, D., Simmons, A., Soci, C., Dee, D., Thépaut, J-N. ERA5 hourly time-series data on single levels from 1940 to present. Copernicus Climate Change Service (C3S) Climate Data Store (CDS). [https://cds.climate.copernicus.eu/datasets/reanalysis-era5-single-levels-timeseries] Accessed 2026-01-30 (2025).

ARTICLE IN PRESS